行政院國家科學委員會補助專題研究計畫 期中進度報告

液態鎵熱力學及結構之研究(1/2)

計畫類別：個別型計畫
計畫編號：NSC　97－2112－M－009－0005－MY2
執行期間：　97 年 8 月 1 日 至 99 年 7 月 31 日

計畫主持人：吳天鳴
共同主持人：
計畫參與人員： 蔡昆憲

成果報告類型(依經費核定清單規定繳交)：精簡報告

執行單位：交通大學物理研究所

中　華　民　國　97 年 5 月 25 日

中文摘要

在流體熱力學微擾理論中，多利用硬球流體做參考系統，再加上粒子間吸力做微擾，以計算流體的自由能。這是過去 Mansoori-Canfield 及 Rasaiah-Stell(MCRS)理論所用的方法。在硬球粒子間所禁止的相空間部分應對流體的自由能有貢獻；這貢獻對非常軟的粒子流體應是特別明顯。最近，依據 MCRS 理論對軟粒子流體的熱力學微擾理論已被提出，而計算的結果和直接從電腦模擬的結果非常符合，數據非常接近。

在一液態鎵的位能模型，兩鎵離子間的作用力包括短程的斥力與長程的 Friedel 振盪位能，而此短程的斥力是非常“軟”的。此計劃的第一部份，是利用此修正的 MCRS 理論計算液態鎵的熱力學函數，其一目的是用此液態鎵的位能模型檢驗此新的軟粒子流體熱力學微擾理論。此一成果已發表於 Journal of Chemical Physics, Vol. 129, 024503 (2008)。詳細內容請參閱所付的論文。

關鍵詞： 微擾理論、硬球流體，軟粒子流體、液態鎵。

Hard-sphere perturbation theory for a model of liquid Ga

K. H. Tsai[1] and Ten-Ming Wu[2,a)]
[1]*Department of Electrophysics, National Chiao-Tung University, HsinChu, Taiwan 300, Republic of China*
[2]*Institute of Physics, National Chiao-Tung University, HsinChu, Taiwan 300, Republic of China*

(Received 22 April 2008; accepted 30 May 2008; published online 8 July 2008)

Investigating thermodynamic properties of a model for liquid Ga, we have extended the application of the hard-sphere (HS) perturbation theory to an interatomic pair potential that possesses a soft repulsive core and a long-range oscillatory part. The model is interesting for displaying a discontinuous jump on the main-peak position of the radial distribution function at some critical density. At densities less than this critical value, the effective HS diameter of the model, estimated by the variational HS perturbation theory, has a substantial reduction with increasing density. Thus, the density dependence of the packing fraction of the HS reference fluid has an anomalous behavior, with a negative slope, within a density region below the critical density. By adding a correction term originally proposed by Mon to remedy the inherent deficiency of the HS perturbation theory, the extended Mansoori–Canfield/Rasaiah–Stell theory [J. Chem. Phys. **120**, 4844 (2004)] very accurately predicts the Helmholtz free energy and entropy of the model, including an excess entropy anomaly. Almost occurring in the same density region, the excess entropy anomaly is found to be associated with the anomalous packing faction of the HS fluid. © *2008 American Institute of Physics*. [DOI: 10.1063/1.2948950]

I. INTRODUCTION

A general realization about simple liquids is that the liquid structure is primarily determined by the repulsive core of particles, while the attractions between particles determine the cohesion of the liquid.[1] Since the repulsions and attractions in a liquid play different roles in thermodynamics of the liquid, the two portions of interatomic interactions are individually approximated with different strategies. The structure of a liquid can be described by a reference fluid with the repulsive core only, whereas the attractions are treated as a perturbation. This forms the central theme of thermodynamic perturbation theory, which has played an important role in the development of statistical mechanism for simple liquids.[2,3] Some refinements of the theory progress recently, with an aim of applications in soft condensed systems.[4–9]

Owing to the benefit of available analytical expressions of the hard-sphere (HS) fluid in calculating thermodynamic and structural properties, the reference fluid is further approximated to be a HS one with the HS diameter determined by requiring that the two fluids are equivalent in some thermodynamic quantity. For example, in the Weeks–Chandler–Andersen (WCA) theory,[10–13] the HS diameter is determined by the equation of equal compressibility between the two fluids so that their free energies differ in the fourth order of the softness parameter, which is a measure for the difference between the repulsive core and the HS potential. Generally, the WCA theory is accurate for the Lennard-Jones (LJ) fluids at high densities. However, as the repulsive core is very soft, the softness parameter is so large that the inaccuracy of the WCA theory becomes serious. With a different choice for the HS diameter, Lado[14] gave some improvement in the prediction of the WCA theory. Alternatively, according to the Gibbs–Bogolubov inequality, Mansoori–Canfield[15] and Rasaiah–Stell[16] (MCRS) developed independently a variational approach, based on a HS reference system and the first-order perturbation. By treating the HS diameter as a variational parameter, this approach provides an upper bound of the Helmholtz free energy. As the repulsive core is softer than that of the LJ potential, the prediction of this variational approach is found to be more accurate than that of the WCA theory. This variational HS perturbation theory has been applied to calculate the structures and thermodynamics of liquid metals, which can be described by the effective pair potentials with very soft repulsive cores.[17–20]

Pointed out by Mon[21–23] in a few years ago, the inaccuracy of the HS perturbation theory is resulted from an inherent deficiency of the theory: A region in the phase space of a realistic fluid is forbidden by a HS fluid due to the singularity of the HS potential. To make up the deficiency of the HS perturbation theory, Mon proposed a correction term that should be added into the variational function to improve the accuracy of the variational approach. By testing the corrected variational function with the inversed-power fluids and a model of liquid Na,[24] the deficiency of the HS perturbation theory is accounted. Recently, including Mon's correction term in the two-body approximation, Ben-Amotz and Stell have extended the MCRS theory.[25] Different from other HS perturbation theories, this extended theory needs two effective HS diameters. The cavity distribution function of a HS fluid, which is in the correction term, is evaluated by the HS-diameter value determined by the Lado-WCA method; other HS-diameter parameters, appearing either explicitly or implicitly in the variational function, are still treated as the variational parameter. Also tested with the inversed-power

a)Author to whom correspondence should be addressed. Electronic mail: tmw@faculty.nctu.edu.tw.

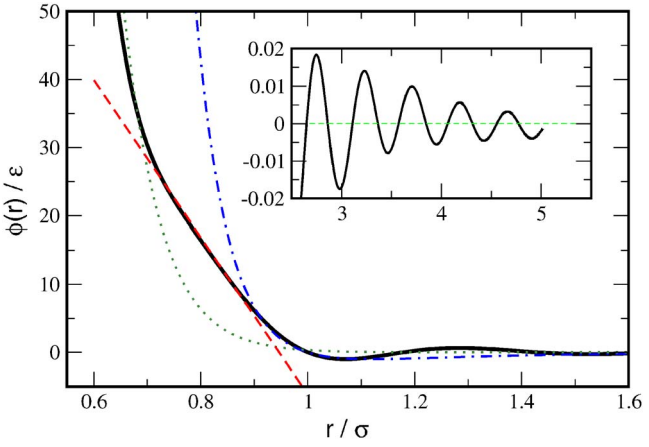

FIG. 1. (Color online) Interatomic pair potential $\phi(r)$ (solid line). The dot-dashed line is the LJ potential with the same ε and σ. The dashed line is a linear function $a_1(r/\sigma)+a_2$ with $a_1=-115\varepsilon$ and $a_2=109\varepsilon$; the dotted line is the function $c_1 \exp(-c_2 r/\sigma)(r/\sigma)^{c_3}$, where $c_1=4.42\times10^6\varepsilon$, $c_2=16.4$, and $c_3=1.5$. The inset shows the oscillatory part of $\phi(r)$ at large distances.

fluids, the extended-MCRS (E-MCRS) theory gives more accurate predictions than other first-order HS perturbation theories.

In terms of an interatomic pair potential generated by a first-principles pseudopotential theory,[26] the structural and dynamic properties of liquid Ga close to the triple point are well described, including the well-known shoulder in static structure factor and the anomaly in the linewidth function of dynamic structure factors at high wavevectors.[27] This interatomic pair potential is characterized by two features: a ledge-shape repulsive core and the long-range oscillations induced by conduction electrons. Although generated numerically, the interatomic pair potential is continuous and smooth, and the behavior of the repulsive core is generally like the two-scale Jagla potential,[28] which have been used to investigate the waterlike anomalies.[29–31] It is interesting to examine the accuracy of the HS perturbation theories mentioned above with this liquid-Ga model, by comparing their predictions with the simulation results. We also estimate the effective HS diameter of this model fluid by these perturbation theories and compare their density variations. We find that the E-MCRS theory gives extraordinarily accurate predictions on the thermodynamic properties of this model from low to high densities, including an excess entropy anomaly at intermediate densities. In the next section, we briefly outline the MCRS and E-MCRS theories. In Sec. III, our model is described and the conditions of our simulations are given. In Sec. IV, we present the calculated results. Our conclusions are given in Sec. V.

II. THEORETICAL BACKGROUND

The excess Helmholtz free energy A^{ex} of a fluid is defined as the difference between the total free energy of the fluid and that of an ideal gas at the same number density ρ and temperature T. A^{ex} is attributed to interactions between particles. Here, we give two methods for how A^{ex} is calculated. The first method is based on the HS perturbation theory and the second is evaluated by a thermodynamic integration of pressure.

Relative to a reference fluid of HSs with diameter σ_{HS} at the same temperature and number density, $\tilde{A}=A^{\mathrm{ex}}/Nk_BT$ of a fluid with N particles can be expressed as

$$\tilde{A} = \tilde{A}_{\mathrm{HS}} + \Delta\tilde{A}, \tag{1}$$

where $\tilde{A}_{\mathrm{HS}}=A^{\mathrm{ex}}_{\mathrm{HS}}/Nk_BT$ is the corresponding quantity of the HS fluid and $\Delta\tilde{A}$ is the difference. $\tilde{A}_{\mathrm{HS}}$ is well described by the Carnahan–Starling expression,[32]

$$\tilde{A}_{\mathrm{HS}} = \frac{\eta(4-3\eta)}{(1-\eta)^2}, \tag{2}$$

where $\eta=\pi\rho\sigma^3_{\mathrm{HS}}/6$ is the packing fraction of the HS fluid. In the MCRS theory,[15,16] $\Delta\tilde{A}$ of a fluid with a pair potential $\phi(r)$ is given as

$$\Delta\tilde{A} \approx 2\pi\rho\beta\int_{\sigma_{\mathrm{HS}}}^{\infty} g_{\mathrm{HS}}(r)\phi(r)r^2dr, \tag{3}$$

where $g_{\mathrm{HS}}(r)$ is the radial distribution function of the HS fluid and $\beta=(k_BT)^{-1}$. By treating σ_{HS} as a variational parameter, a measured value of $\tilde{A}$ is obtained by minimizing a sum of $\tilde{A}_{\mathrm{HS}}$ and $\Delta\tilde{A}$ given in Eqs. (2) and (3), respectively.

In principle, the entire configuration space Ω is accessible to a realistic fluid. Because of the singularity of a HS potential, part of Ω is not available to the HS fluid, which configuration space is denoted as Ω_{HS}. This is due to the excluded volume effect of the HS particles. Mon pointed out that due to the difference between Ω_{HS} and Ω a correction term that should be added into $\Delta\tilde{A}$ is formulated as[21–23]

$$\Delta_\eta = \frac{1}{N}\ln\left[\frac{\int_{\Omega_{\mathrm{HS}}} e^{-\beta\Phi}}{\int_{\Omega} e^{-\beta\Phi}}\right], \tag{4}$$

where Φ is the total interaction energy of the fluid of interest.

To the lowest order of fluid density, Ben-Amotz and Stell have shown that the correction term can be approximated to be[25]

$$\Delta_\eta = -2\pi\rho\int_0^{\sigma_{\mathrm{HS}}} g(r)r^2dr, \tag{5}$$

where $g(r)$ is the radial distribution function of the fluid with $\phi(r)$. As commonly used in the HS perturbation theory, $g(r)$ in the repulsive-core region is approximated as

$$g(r) = y_{\mathrm{HS}}(r)\exp(-\beta\phi(r)), \tag{6}$$

where $y_{\mathrm{HS}}(r)$ is the cavity distribution function of the HS reference fluid. By using this approximation, a new variational formula of $\Delta\tilde{A}$, refereed as the E-MCRS theory, is given as

$$\Delta\tilde{A} = 2\pi\rho\beta\int_{\sigma_{\mathrm{HS}}}^{\infty} g_{\mathrm{HS}}(r)\phi(r)r^2dr - 2\pi\rho\int_0^{\sigma_{\mathrm{HS}}} y_{\mathrm{HS}}(r)\exp(-\beta\phi(r))r^2dr. \tag{7}$$

It has been shown that the E-MCRS theory gives better predictions in thermodynamic properties of the inverse-power fluids than other first-order HS perturbation theories. How-

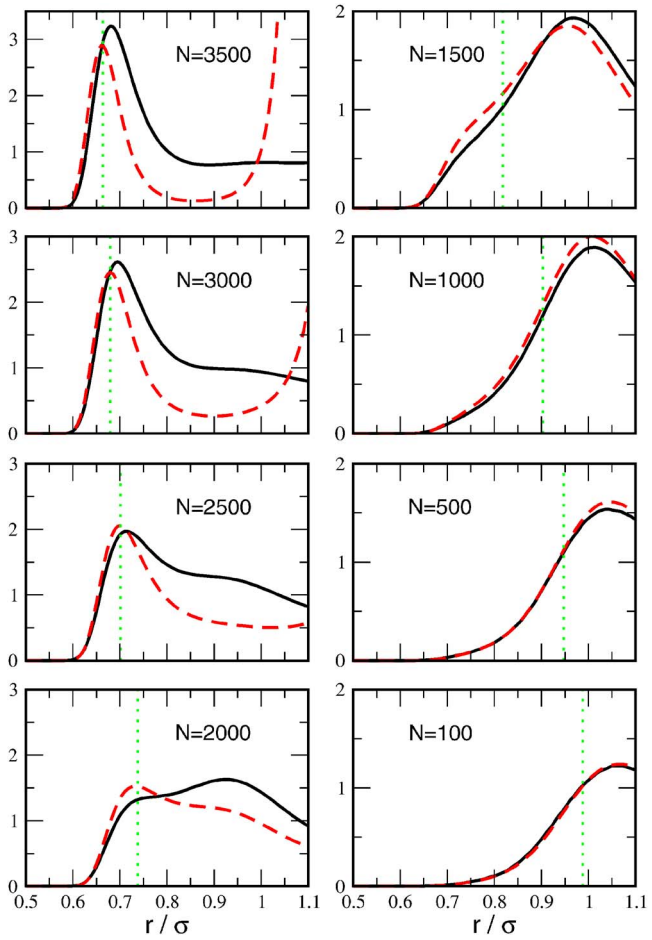

FIG. 2. (Color online) Radial distribution function of the model fluid at the indicated particle number. In each panel, the solid and dashed lines are, respectively, the simulation result and the approximation given by Eq. (6) with $y_{HS}(r)$ evaluated at the Lado-WCA value of σ_{HS}. The dotted line indicates the σ_{HS} value obtained by the E-MCRS theory.

ever, a notice should be given: The HS diameter for describing $y_{HS}(r)$ in the second integral is determined by the Lado-WCA method and may have a different value from that of the variational parameter σ_{HS}, which implicitly determines $g_{HS}(r)$ in the integrand of the first integral and appears explicitly in the lower and upper limits of the first and second integrals, respectively.

In thermodynamics, $\tilde{A}$ of a fluid at density ρ is related to the pressure $P(\rho')$ of the fluid at lower density ρ' via the following integration:[2]

$$\tilde{A} = \int_0^{\rho} \left(\frac{\beta P(\rho')}{\rho'} - 1 \right) \frac{d\rho'}{\rho'}. \tag{8}$$

$P(\rho')$ can be obtained via the pressure equation, in which two inputs are the radial distribution function of the fluid at density ρ' and the first derivative of the pair potential. With the radial distribution functions generated by computer simulation, $\tilde{A}$ obtained via the integration in Eq. (8) is recognized as the simulation results, which have no approximations in thermodynamics.

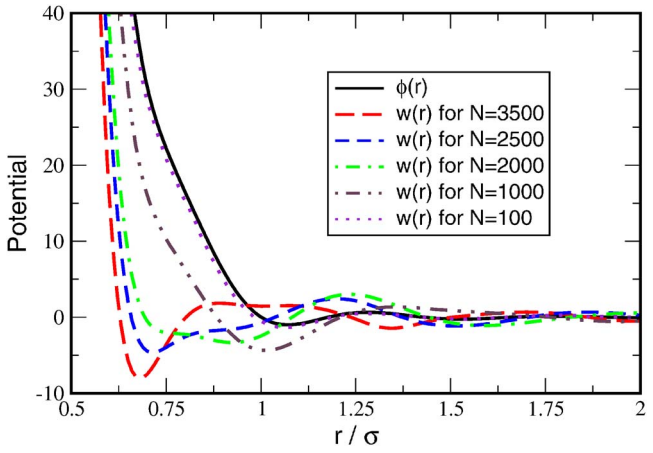

FIG. 3. (Color online) Potential of mean force $w(r)$ of the model fluid at $N=3500$ (dashed line), 2500 (short-dashed line), 2000 (dot-dashed line), 1000 (dot-dot-dashed line), and 100 (dotted line). The solid line is the interatomic pair potential $\phi(r)$. All potentials are scaled with ε and distance is scaled with σ.

III. MODEL OF LIQUID Ga AND SIMULATIONS

The interatomic pair potential $\phi(r)$ used in this paper is generated by a first-principles pseudopotential theory for liquid Ga at $T=323$ K.[26] Although the numerical data of $\phi(r)$ are generated at discrete points, the overall shape of $\phi(r)$, shown in Fig. 1, is continuous and smooth. Generally, $\phi(r)$ has a ledge-shape repulsive core and a long-range oscillatory part with a behavior following the Friedel oscillations.[27] Two parameters of $\phi(r)$ are ε, the depth of the main attractive well, and σ, which is the shortest distance at $\phi(r)=0$. The corresponding temperature of ε is about 47 K and $\sigma=4.04$ Å. The repulsive core of $\phi(r)$, denoted as $\phi_0(r)$, is the potential for r smaller than r_0, the position of the main attractive well, where r_0 is about 1.07σ. According to the behavior of the repulsive core, $\phi_0(r)$ can be roughly divided into three sections. As r is larger than 0.9σ, $\phi_0(r)$ with energy less than 6ε behaves like the repulsive core of the LJ potential with the same σ and ε.[33] In the intermediate region between 0.9σ and 0.7σ, the value of $\phi_0(r)$ varies from 6ε to 30ε and the shape of $\phi_0(r)$ becomes soft and has a ramplike behavior, with a reflection point around 0.8σ.[34] At r less than 0.7σ, $\phi_0(r)$ increases almost exponentially with decreasing distance so that the repulsive core changes to be extremely stiff.

With $\phi(r)$, we have carried out a series of molecular dynamics simulations at constant *NVE* ensemble by using a predictor-corrector algorithm[35] in a time step of 5.45 fs. In each simulation, the temperature is set to be 6.85ε, corresponding to $T=323$ K, the box size is fixed at 10.2σ, and the range of $\phi(r)$ is terminated at half of the box size. All quantities given in this paper are in units of σ, ε and the mass of Ga atom. The number of simulated particles starts at $N=3500$. Then, in each simulation for a new thermodynamic state, N is reduced by 100, with the lowest N being 100. At $N=3500$, the simulated system has a number density $\rho=0.05$ Å^{-3}, with a reduced density $\rho^* \equiv \rho\sigma^3$ equal to 3.305, which is close to that of liquid Ga at $T=323$ K and pressure of about 1 bar. At the simulated conditions of $N=3500$, the

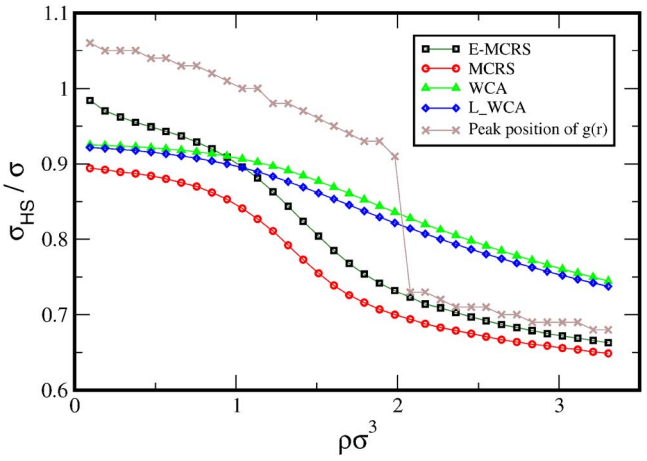

FIG. 4. (Color online) Effective HS diameter σ_{HS} as a function of density. σ_{HS} is estimated by various theories: WCA (triangles), Lado-WCA (diamonds), MCRS (circles), and E-MCRS (squares). The crosses stand for the main-peak position of $g(r)$. The symbols of each kind are connected by a line to guide the eye.

static and dynamic structure factors of the system reproduce well the experimentally observed structural and dynamic anomalies of liquid Ga at temperatures close to the melting point (T_m=303 K).[27]

The radial distribution functions of our simulated systems at some particle numbers are shown in Fig. 2. At N=3500, the main peak of the radial distribution function is located at 0.686σ, which is in the extremely stiff region of the repulsive core. As N is decreased, the main peak is lowered and shifts outwardly, while a shoulder near σ appears and then grows. Around N=2100, corresponding to $\rho^* \approx 2$, the roles of the main peak and the shoulder exchange: the main peak changes to occur near σ and the shoulder resides in the inner part of the repulsive core. As N keeps on decreasing, the inner shoulder gradually disappears, associated with a continuously growing main peak near σ as a compensation. As N is less than 1000, the number density of the system is rather low and the main peak moves toward the first attractive well, with a final position located at the minimum of the attractive well. A similar density variation of the radial distribution function is also observed for the one-scale and two-scale ramp potentials[31] introduced by Jagla[28] and the core-softened continuous potential with an attractive well.[36]

Another way to manifest the density effect on the radial distribution function of this model is to compare the potential of mean force, which is defined as $w(r)=-k_BT \ln g(r)$, with $\phi(r)$. $w(r)$ is the potential that gives the mean force acting on a particle in the fluid. In concept, the mean force between two neighboring particles in a dense fluid includes the direct force due to the interatomic pair potential and an effective force indirectly intermediated through other particles. In general, the indirect force depends on the fluid density, so the potential of mean force at high density can be quite different from the interatomic pair potential. For our model fluid, the variation of $w(r)$ with N is presented in Fig. 3. At N=3500, $w(r)$ has a deep attractive well at the first-peak position of $g(r)$; this attractive well is attributed to the compactness in the fluid at such a high density. As N is decreased, the depth of this attractive well gradually reduces, while a shoulder near σ appears. At some critical N, corresponding to a critical density, the roles of this attractive well and the shoulder in $w(r)$ switch with each other. As N is decreased further, the new attractive well in $w(r)$ continuously moves out, with its depth becoming deeper first and then attenuated to ε at final.

In the WCA theory,[11] the effective σ_{HS} of the model is determined by the solution of the following integral equation:

$$\int_0^{r_0} y_{HS}(r)\exp(-\beta\phi_0(r))r^2dr = \int_{\sigma_{HS}}^{r_0} y_{HS}(r)r^2dr. \quad (9)$$

This integral equation implies equal compressibility between the reference fluid with the repulsive core $\phi_0(r)$ and the fluid of HSs with diameter σ_{HS} at the same temperature and density. In the Lado-WCA method,[14] the effective HS diameter is given by the solution of a similar equation, by replacing $y_{HS}(r)$ in both integrands in Eq. (9) with $\partial y_{HS}(r)/\partial\sigma_{HS}$. To solve these equations efficiently, we have replaced $y_{HS}(r)$ and $\partial y_{HS}(r)/\partial\sigma_{HS}$ with their analytical expressions in the hard-fluid (HF) approximation,[37,38] which can be simply evaluated in terms of the packing fraction η of the HS fluid.

By using the discrete data of $\phi_0(r)$ and η evaluated at the simulated density, we have solved these equations to obtain the WCA and Lado-WCA values of HS diameter, and their density variations are shown in Fig. 4. For each method, our results are consistent with the general understanding that the effective HS diameter of a fluid is decreased with increasing the fluid density.[25] At each density, the HS diameters obtained by the two methods are close, with the WCA value larger. At high densities, both WCA and Lado-WCA σ_{HS} values are larger than the main-peak position of $g(r)$, which is located in the exponential region of the repulsive core. But, the HS diameters estimated at low densities becomes smaller than the main-peak position of $g(r)$, which has a sudden jump to a larger distance in the repulsive core with a LJ-type behavior around ρ^*=2. With the results shown in Fig. 2 for some particle numbers, we have examined the approximated $g(r)$ given in Eq. (6) for our model, with $y_{HS}(r)$ evaluated in the HF approximation at the Lado-WCA value of HS diameter. For our model at high densities, Eq. (6) is a good approximation of $g(r)$ for distances less than the main-peak position, while at low densities the validity of the approximation extends over the main peak of $g(r)$.

IV. THERMODYNAMIC PROPERTIES

Through the pressure equation with $g(r)$ generated by our simulations as an input, we have calculated the compressibility factor $Z \equiv \beta P(\rho)/\rho$ of our model and the results are shown by the symbols in Fig. 5. Theoretically, $Z(\rho)$ as a function of density can be expanded into a series with the leading term to be one.

$$Z(\rho) = 1 + b_2\rho + b_3\rho^2 + b_4\rho^3 + b_5\rho^4 + \cdots. \quad (10)$$

Here, b_i is the ith Virial coefficient, which is associated with $\phi(r)$ via some diagrams.[2] In the second Virial approximation, $Z(\rho)$ is approximated to be $1+b_2\rho$ and the calculation of b_2 is

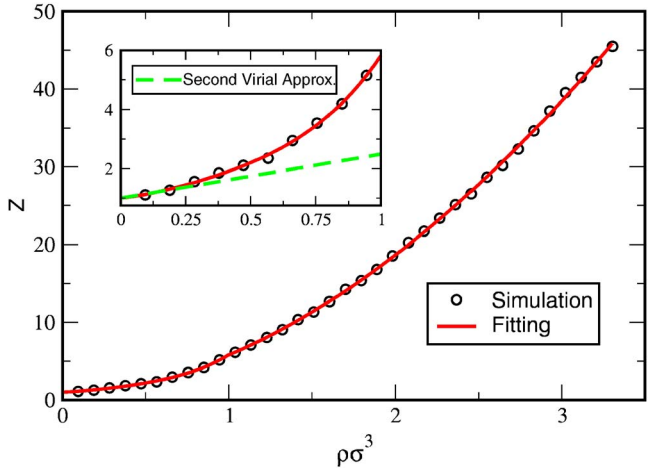

FIG. 5. (Color online) Compressibility factor, $Z=\beta P/\rho$, as a function of density. The circles are calculated by the pressure equation with the simulated $g(r)$ as an input. The solid line is the fitting function as described in the text with the fitting parameters given in Table I. The inset shows Z at low densities and the second Virial approximation (dashed line).

straightforward. Shown in the inset of Fig. 5 is the second Virial approximation of our model, which serves as a check for the accuracy of our calculations at low densities. In order to perform numerical integration in Eq. (8), we fit $Z(\rho)$ in Fig. 5 with the series in Eq. (10) truncated beyond the fourth order of ρ and treat the Virial coefficients as fitting parameters. To make the fitting accurate enough, the data of $Z(\rho)$ for ρ^* larger and smaller than 1 are fitted separately and the values of the fitting parameters are given in Table I. Although the fitting function has an unnoticed discontinuity at $\rho^*=1$, this discontinuity has little effect on the numerical values of $\tilde{A}$ at higher densities. By using the fitting function of $Z(\rho)$, we have done the integration in Eq. (8) and the calculated $\tilde{A}$ are indicated by the symbols in Fig. 7.

In the MCRS and E-MCRS theories, the variational $\tilde{A}$ is minimized with σ_{HS} as the only variational parameter. During the minimization process, $g_{\mathrm{HS}}(r)$ in the integral in Eqs. (3) and (7) is generated by the Verlet algorithm,[39] and $y_{\mathrm{HS}}(r)$ in the second integral in Eq. (7) is replaced by the analytical expression of the HF approximation[37,38] with the Lado-WCA σ_{HS} value. Shown in Fig. 6 are the variational curves of $\tilde{A}$ at some particle numbers. For each curve, the values of $\tilde{A}$ and the effective HS diameter at the minimum are determined numerically. Since the value of Mon's correction term decreases with increasing σ_{HS}, adding this correction term into the variational function causes the minimum of the variational curve shifting to a lower value of excess free energy and a larger value of effective HS diameter. Thus, for all thermodynamic states, the E-MCRS theory gives a better prediction on the excess Helmholtz free energy than the MCRS theory does, and the value of the HS diameter obtained by the E-MCRS theory is larger than that by the MCRS theory. These results are expected to be true for all kinds of fluid.[25]

TABLE I. The fitting coefficients of $Z(\rho)$ for $\rho^*<1$ and $\rho^*>1$. The data are given in unit of σ.

$Z(\rho)$	b_2	b_3	b_4	b_5
$\rho^*<1$	0.995	4.129	−4.969	4.670
$\rho^*>1$	−0.323	5.228	−0.523	0.055

In order to investigate the effect of the approximation in Eq. (6) on the values predicted by the E-MCRS theory, we also evaluate the variational $\tilde{A}$ with Mon's correction term Δ_η given in Eq. (5) with the simulated $g(r)$ used. As shown in Fig. 6, the corresponding variational curve of $\tilde{A}$ generally shifts upward relative to the one obtained by the E-MCRS theory, except that at very low densities the curves of the two methods are found to be almost the same. Therefore, our results lead to the conclusion that the approximation in Eq. (6) makes the prediction of the E-MCRS theory better.

In Fig. 4, the density variations of the effective HS diameters obtained by the MCRS and E-MCRS theories are compared to those obtained by the WCA and Lado-WCA theories. Similar as the results of the WCA and Lado-WCA theories, the σ_{HS} values estimated by the MCRS and E-MCRS theories also increase with decreasing density. For ρ^* larger than 2, the σ_{HS} values of the MCRS and E-MCRS theories are limited by the main-peak position of $g(r)$, with the density dependence of the E-MCRS value almost along the track of the peak position. For ρ^* less than 2 around which the main-peak position of $g(r)$ makes a jump to a larger value, the MCRS and E-MCRS values are apparently released from the restriction due to the main-peak position of $g(r)$ and ascend manifestly as ρ^* varies from 2 to 1. For ρ^* less than 1, the MCRS value becomes saturated roughly to 0.9σ as density approaches to zero, but the E-MCRS value continuously increases at very low densities and even passes over the values of the WCA and Lado-WCA theories.

The comparison of the excess Helmholtz free energies estimated by various HS perturbation theories is shown in Fig. 7. Apparently, the variational approaches do a better job than the WCA and Lado-WCA theories, which are only good for ρ^* less than 1. For all calculated densities, the predicted value of the E-MCRS theory is the one closest to the simulation data.

The excess entropy S^{ex} of a realistic fluid is defined as the difference between the entropy of the fluid and that of an ideal gas at the same density and temperature. In thermodynamics,

$$S^{\mathrm{ex}} = -(\partial A^{\mathrm{ex}}/\partial T)_{N,V}. \tag{11}$$

$\tilde{S}$ is defined as S^{ex}/Nk_B. In the MCRS theory, the excess entropy $\tilde{S}_{\mathrm{MCRS}}$ is equal to $-\tilde{A}_{\mathrm{HS}}$, which is the excess entropy of a HS fluid with the HS diameter of the MCRS value.[19] In the E-MCRS theory, Mon's correction term gives an extra contribution to $\tilde{S}$. In order to derive the extra contribution, we use the formula of Δ_η in Eq. (5), rather than the approximated one in Eq. (7). After substituting $g(r)=\exp(-\beta w(r))$ into Eq. (5), $\tilde{S}$ in the E-MCRS theory can be expressed as

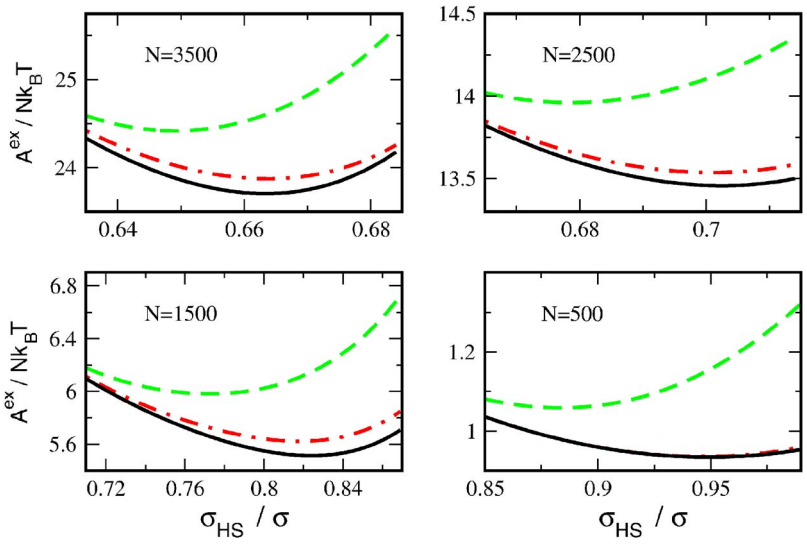

FIG. 6. (Color online) Variational $\tilde{A}$ as a function of σ_{HS} at the indicated particle number. In each panel, the solid and dashed lines are the E-MCRS and MCRS $\tilde{A}$, respectively. The dot-dashed line is the variational $\tilde{A}$ with Mon's correction term given in Eq. (5). For $N=500$, the solid and dot-dashed lines are almost the same.

$$\tilde{S}_{\mathrm{EMCRS}} = -\tilde{A}_{\mathrm{HS}} + 2\pi\rho \int_0^{\sigma_{\mathrm{HS}}} g(r)[1+\beta w(r)]r^2 dr. \quad (12)$$

Here, the second term on the right-hand side is due to Mon's correction term. Then, after using the approximation in Eq. (6) for $g(r)$,

$$\tilde{S}_{\mathrm{EMCRS}} = -\tilde{A}_{\mathrm{HS}} + 2\pi\rho \int_0^{\sigma_{\mathrm{HS}}} y_{\mathrm{HS}}(r)\exp(-\beta\phi(r)) \times[1+\beta\phi(r)-\ln y_{\mathrm{HS}}(r)]r^2 dr. \quad (13)$$

To evaluate $\tilde{S}_{\mathrm{EMCRS}}$, the HS diameter is required in three places in the above equation: the packing fraction in $\tilde{A}_{\mathrm{HS}}$, the upper limit of the integral in the second term, and $y_{\mathrm{HS}}(r)$, which is approximated to be the analytical expression of the HF approximation.[37,38] Care must be taken for that the value of σ_{HS} in the first and second places should be the one obtained by the minimization of variational $\tilde{A}$ in the E-MCRS theory but the Lado-WCA value of σ_{HS} should be used in the third place. Also, we have calculated Eq. (12) in terms of the simulated $g(r)$ and $w(r)$, and no significant difference is found between the results calculated by Eqs. (12) and (13). Thus, for our model, the two equations give almost identical results.

On the other hand, $\tilde{S}$ can be evaluated by the difference between the excess internal energy $\tilde{U}$ and the $\tilde{A}$ obtained by Eq. (8). By using $\phi(r)$ and the simulated $g(r)$, the calculation of $\tilde{U}$ is straightforward[2] and the result of $\tilde{S}$ is shown by the symbols in Fig. 8. The value of $\tilde{S}$ at $\rho^*=3.305$ is estimated to be −4.10, which is reasonably comparable to the experimental value of −4.62 of the excess entropy of liquid Ga at a higher temperature.[19] At low densities, $\tilde{S}$ decreases almost linearly with density; this decrease arises from the excluded volume effect due to the repulsive core of $\phi(r)$. Intriguingly, in the intermediate range of density, roughly from $\rho^*=1.4$ to 1.8, the density curve of $\tilde{S}$ has an anomalous behavior, which has a positive slope of a small value. Beyond this anomalous region, $\tilde{S}$ decreases again in a slower rate with increasing density. Observed also in the two-scale ramp potential,[40] the

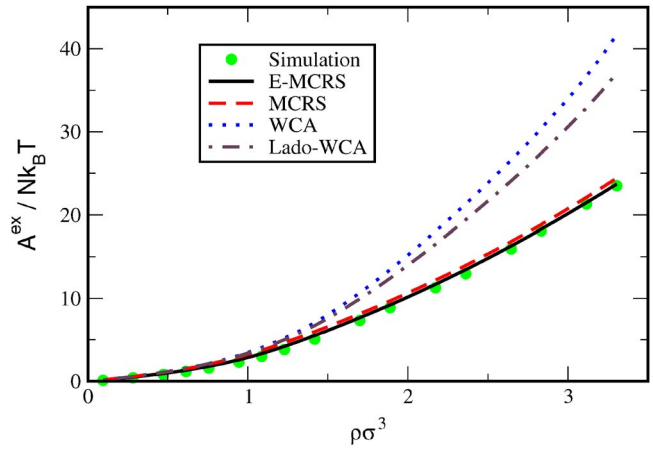

FIG. 7. (Color online) The excess Helmholtz free energy $\tilde{A}=A^{\mathrm{ex}}/Nk_BT$ predicted by the E-MCRS (solid line), MCRS (dash line), WCA (dotted line), and Lado-WCA (dot-dashed line) theories and the results calculated by thermodynamic integration in Eq. (8) (symbols).

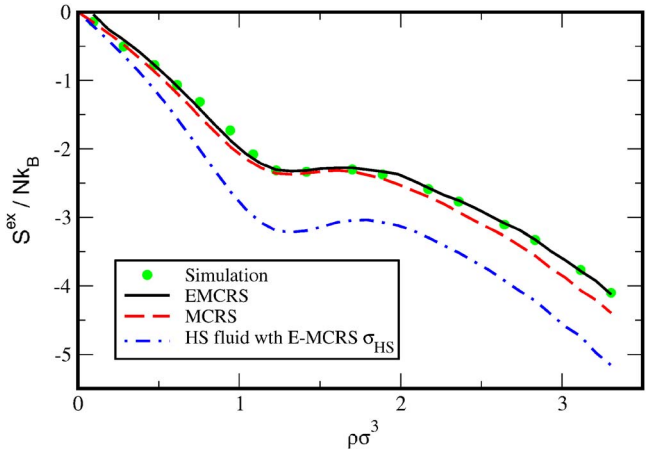

FIG. 8. (Color online) Density dependence of the excess entropy S^{ex}/Nk_B. The solid and dashed lines are the predictions of the E-MCRS and MCRS theories, respectively. The dot-dashed line is the excess entropy of the HS fluid with the HS diameter estimated by the E-MCRS theory. The symbols are the simulated results as described in the text.

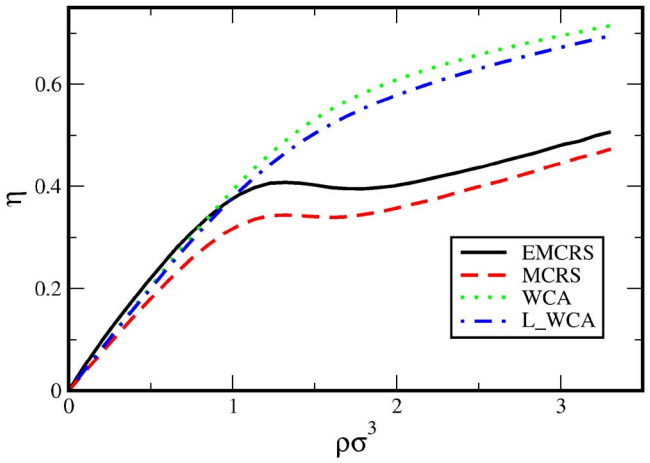

FIG. 9. (Color online) Density dependence of packing fraction η of the HS fluid with the E-MCRS (solid line), MCRS (dashed line), WCA (dotted line), and L-WCA (dot-dashed line) σ_{HS} values shown in Fig. 4.

anomalous behavior of $\tilde{S}$ is associated with the density anomaly, where the density increases with increasing temperature at constant pressure.[41]

For our model, the comparison between $\tilde{S}$ calculated by simulation and those obtained by the MCRS and E-MCRS theories is shown in Fig. 8; the three results of $\tilde{S}$ give similar density behavior. The predictions of the MCRS theory agree with the simulation results only at low densities and produce an excess entropy anomaly in a range shifting a little toward smaller density, but are deviated from the simulation data at densities beyond the anomalous region. The E-MCRS theory has a triumph over the MCRS theory for a perfect agreement with the simulation results in the entire range of density we have calculated. We also present the excess entropy of the HS fluid with the E-MCRS HS diameter, which shows a manifested anomaly with a larger positive slope. The absolute value of the excess entropy of this HS fluid is larger than that estimated by the E-MCRS theory. This implies that because part of the phase space is inaccessible by the HS fluid, in which the free volume of each particle is reduced, the difference between the entropy of the HS fluid and that of the ideal gas is, therefore, enhanced. Mon's correction makes a compensation for the excluded volume effect so that the predictions of the E-MCRS theory for all densities agree well with the simulation results. As indicated in Fig. 8, the larger the fluid density is, the more significant the compensation due to Mon's correction term. Thus, Mon's correction fundamentally improves the prediction of the HS variational approach for the excess entropy of a fluid.

To address the reason why the anomaly in $\tilde{S}$ predicted by the MCRS and E-MCRS theories occurs in our model, we have plotted in Fig. 9 the density dependence of the packing fractions of the reference HS fluids in various perturbation theories. In the WCA or the Lado-WCA theories, the packing faction η increases monotonically with the increase in density. At $\rho^*=3.3$, which is close to that of realistic liquid Ga, the η values estimated by the two theories are over 0.7, which is in the solid phase of a HS system. This indicates that because of the overestimation in the effective HS diameter, the reference HS fluids in the two theories are too much deviated from our model. On the other hand, with the σ_{HS} values estimated by the MCRS and E-MCRS theories, the density curve of the packing fraction apparently has a negative slope in the intermediate region, roughly from $\rho^*=1.3$ to 1.7, which corresponds to the substantial shrinkage in the size of the effective HS with increasing density, as shown in Fig. 4. Thus, the packing fraction of the HS fluid is reduced with increasing density in this density region. This anomaly in the packing fraction is the origin for the excess entropy anomaly predicted by the two theories. Beyond this anomalous region in packing fraction, the size of the effective HS is limited by the exponentially increasing repulsion in the inner core of the pair potential so that the packing fraction increases again with density at a smaller rate. At $\rho^*=3.3$, the packing fractions estimated by the MCRS and E-MCRS theories are, respectively, 0.473 and 0.5, which are in the fluid-solid coexistence region of the HS system, and the reference HS system is physically reasonable.

V. CONCLUSIONS

In terms of various HS perturbation theories, we have investigated thermodynamic behaviors of a model fluid, with which the structure and dynamic properties of liquid Ga close to the triple point are reproduced.[26,27] The interatomic pair potential of the model has two features: a ledge-shape repulsive core and a long-range oscillatory part. Somewhat like the two-scale ramp potential,[31,32] the repulsive core of the pair potential varies continuously from an exponential-decay inner core, through a ramplike intermediate region, to a LJ-type outer core. The model has been simulated at constant *NVE* conditions from low to high densities; at the highest density the simulated system corresponds to realistic liquid Ga at $T=323$ K. The radial distribution function of the model has an interesting variation with number density: At high density, the main peak of the radial distribution function is located in the inner region of the repulsive core with an exponential decay. At some critical density, the position of the main peak makes a discontinuous jump to the outer core of the LJ-type region. As the density is further decreased, the main peak moves toward the minimum of the first attractive well of the pair potential.

We have used the WCA, Lado-WCA, MCRS, and E-MCRS methods to estimate the effective HS diameter of the model. With the HS diameter estimated by the WCA or Lado-WCA method, the packing fraction of the HS system monotonically increases with density and, therefore, the packing fractions at high densities are over the freezing point of the HS system, which makes the WCA and Lado-WCA theories breakdown for our model at high densities. In the MCRS and E-MCRS theories, due to the structural change resulted from the discontinuous jump in the main-peak position of the radial distribution function, the estimated HS diameter is substantially reduced with increasing density, which renders the density curve of the packing fraction having a negative slope in a region of intermediate density. Beyond this negative-slope region, the packing faction of the

HS reference system increases again with density and has a physically reasonable value at high densities.

By including Mon's correction term to compensate the deficiency of the HS perturbation theory, the E-MCRS theory indeed gives better predictions than the MCRS theory does; the predictions of the E-MERS theory for the excess Helmohltz free energy and entropy agree well with the simulation results from low to high densities. The excess entropy of our model is found to have an anomalous behavior, which has a density function with a positive slope. This excess entropy anomaly also occurs in the two-scale ramp potential,[39] with which the waterlike thermodynamic properties are investigated recently.[30,31] The excess entropy anomaly in our model can be described by the E-MCRS and MCRS theories, and the anomaly is associated with the substantial reduction of the effective HS diameter estimated by the two variational theories. Our results indicate that the E-MCRS theory is superior to other first-order HS perturbation theories for investigating thermodynamics of core-softened potentials.

ACKNOWLEDGMENTS

T.M.W. would like to acknowledge financial support from the National Science Council of Taiwan, R. O. C. under Grant No. NSC 95-2112-M-009-027-MY2.

[1] C. Chandler, J. D. Weeks, and H. C. Andersen, Science **220**, 787 (1983).
[2] J. P. Hensen and I. R. McDonald, *Theory of Simple Liquids* (Academic, New York, 1986).
[3] J. A. Barker and D. Henderson, Rev. Mod. Phys. **48**, 587 (1976).
[4] D. Ben-Amotz and G. Stell, J. Phys. Chem. B **108**, 6877 (2004).
[5] F. O. Raineri, G. Stell, and D. Ben-Amotz, J. Phys.: Condens. Matter **16**, S4887 (2004).
[6] S. Zhou, Phys. Rev. E **74**, 031119 (2006).
[7] S. Zhou, J. Chem. Phys. **125**, 144518 (2006).
[8] S. Zhou, J. Phys. Chem. B **111**, 10736 (2007).
[9] A. B. Adib, Phys. Rev. E **75**, 061204 (2007).
[10] D. Chandler and J. D. Weeks, Phys. Rev. Lett. **25**, 149 (1970).
[11] J. D. Weeks, D. Chandler, and H. C. Andersen, J. Chem. Phys. **54**, 5237 (1971).
[12] H. C. Andersen, J. D. Weeks, and D. Chandler, Phys. Rev. A **4**, 1597 (1971).
[13] H. C. Andersen, D. Chandler, and J. D. Weeks, Adv. Chem. Phys. **34**, 105 (1976).
[14] F. Lado, Mol. Phys. **52**, 871 (1984).
[15] G. A. Mansoori and F. B. Canfield, J. Chem. Phys. **51**, 4958 (1969).
[16] J. Rasaiah and G. Stell, Mol. Phys. **18**, 249 (1970).
[17] D. Stroud and N. W. Ashcroft, Phys. Rev. B **5**, 371 (1972).
[18] J. Hafner, Phys. Rev. A **16**, 351 (1977).
[19] R. Kumaravadivel and R. Evans, J. Phys. C **9**, 3877 (1976).
[20] J. Hafner, *From Hamiltonians to Phase Diagrams* (Springer-Verlag, Berlin, 1987).
[21] K. K. Mon, J. Chem. Phys. **112**, 3245 (2000).
[22] K. K. Mon, J. Chem. Phys. **115**, 4766 (2001).
[23] K. K. Mon, J. Chem. Phys. **116**, 9392 (2002).
[24] K. K. Mon, Phys. Rev. E **63**, 061203 (2001).
[25] D. Ben-Amotz and G. Stell, J. Chem. Phys. **120**, 4844 (2004).
[26] S. F. Tsay and S. Wang, Phys. Rev. B **50**, 108 (1994).
[27] K. H. Tsai, T. M. Wu, S. F. Tsay, and T. J. Yang, J. Phys.: Condens. Matter **19**, 205141 (2007).
[28] E. A. Jagla, J. Chem. Phys. **111**, 8980 (1999).
[29] J. R. Errington and P. G. Debenedetti, Nature (London) **409**, 318 (2001).
[30] Z. Yan, S. V. Buldyrev, N. Giovambattista, and H. E. Stanley, Phys. Rev. Lett. **95**, 130604 (2005).
[31] Z. Yan, S. V. Buldyrev, N. Giovambattista, P. G. Debenedetti, and H. E. Stanley, Phys. Rev. E **73**, 051204 (2006).
[32] N. F. Carnahan and K. E. Starling, J. Chem. Phys. **51**, 635 (1969).
[33] T. M. Wu, S. F. Tsay, S. L. Chang, and W. J. Ma, Phys. Rev. B **64**, 064204 (2001).
[34] T. M. Wu, W. J. Ma, S. L. Chang, and S. F. Tsay, Physica B (Amsterdam) **316–317**, 606 (2002).
[35] A. Rahman, Phys. Rev. **136**, A405 (1964).
[36] A. B. de Oliveira, P. A. Netz, T. Colla, and M. C. Barbosa, J. Chem. Phys. **125**, 124503 (2006).
[37] L. E. S. de Souza and D. Ben-Amotz, Mol. Phys. **78**, 137 (1993).
[38] D. Ben-Amotz and G. Stell, J. Chem. Phys. **119**, 10777 (2003); **120**, 4994 (2004).
[39] L. Verlet and J. J. Weiss, Phys. Rev. A **5**, 939 (1972).
[40] J. R. Errington, T. M. Truskett, and J. Mittal, J. Chem. Phys. **125**, 244502 (2006).
[41] R. M. Lynden-Bell and P. G. Debenedetti, J. Phys. Chem. B **109**, 6527 (2005).